Unligated Epidermal Growth Factor Receptor Forms Higher Order Oligomers within Microclusters on A431 Cells That Are Sensitive to Tyrosine Kinase Inhibitor Binding†

Andrew H. A. Clayton,* Maria L. Tavarnesi, and Terrance G. Johns

The Ludwig Institute for Cancer Research, Melbourne Tumour Biology Branch, P.O. Box 2008, Royal Melbourne Hospital, Victoria 3050, Australia, and Melbourne Clinical Sciences, Austin Health, Studley Road, Heidelberg, Victoria 3084, Australia

Received January 2, 2007; Revised Manuscript Received February 22, 2007

ABSTRACT: Characterization of the association states of the unligated epidermal growth factor receptor (EGFR) is important in understanding the mechanism of EGFR tyrosine kinase activation in a tumor cell environment. We analyzed, in detail, the association states of unligated, immunotagged EGFR on the surface of intact epidermoid carcinoma A431 cells, using AlexaFluor488 and AlexaFluor546 anti-EGFR antibody, mAb528, as probes. Image correlation microscopy revealed the presence of unligated EGFR in submicron scale clusters containing an average of 10−30 receptors (mean cluster density = 32 ± 9 clusters per square micron). Lifetime-based Förster resonance energy transfer (FRET) techniques as a function of acceptor:donor labeling ratio disclosed a clustering of the unligated EGFR in clusters containing an average of four receptors on the nanometer (<10 nm) scale. The relationship between the nanoscale and submicron scale associations was determined using a new analysis that combines nanoscale information from lifetime-detected FRET imaging with submicron scale information obtained with image correlation microscopy. This analysis revealed the presence of monomers (or small oligomers) and larger clusters containing 15−30 receptors that were partially associated on the sub-10 nm scale. Pretreatment of the cells with the tyrosine kinase inhibitor AG1478 caused a partial dispersal of the submicron clusters (mean cluster density = 85 ± 15 clusters per square micron; mean degree of association = 4−10 receptors per cluster) and reduced the level of FRET down to our limit of detection. These results are consistent with a higher order nanoscale receptor organization of the unligated receptor population that is partially controlled by the kinase domains. The ramifications of the results to mechanisms of EGFR activation in a tumor cell environment are discussed.

The epidermal growth factor receptor (EGFR)[1] is a member of the epidermal growth factor (EGF) receptor tyrosine kinase family (*1*, *2*). Aberrant signaling from the EGFR network contributes to a number of processes important to cancer development and progression, including cell proliferation, apoptosis, angiogenesis, and metastatic spread. EGFR overexpression and truncation (*1*) have both been observed in common cancers including brain, lung, breast, colon, and prostate, giving credence to the notion that a molecular understanding of EGFR activation in a tumor cell environment will yield opportunities for developing new anticancer drugs (*1*).

The mechanism of activation of the EGFR has been the subject of extensive investigations. Ligand-induced EGFR activation is thought to occur within preformed dimers (*1*, *18*) and/or by ligand-induced dimer formation (*1*−*3*). Three-dimensional structural data (*15*), biochemical cross-linking studies (*16*), single molecule imaging (*17*), and FRET (*18*) studies are usually interpreted in terms of EGFR dimers. On the other hand, studies directed at the cell membrane have revealed a more complex pattern of receptor association. Recent microscopy studies of EGFR expressed at normal levels at the cell surface have shown that ligand-free EGFR is dimeric and undergoes a further oligomerization to form higher order oligomers (tetramers) in the presence of EGF (*31*, *32*). An even higher level of (submicron scale) organization is present on tumorgenic cell lines which overexpress erbB receptors. Image correlation spectroscopy (*19*), phosphorescence anisotropy decay measurements (*20*), and scanning near-field optical microscopy (on erbB2) (*21*) detect higher order clusters containing 10−100 ErbB receptors and spanning hundreds of nanometers. These studies suggest in cell lines overexpressing the receptor that the EGFR is organized both on the submicron and nanometer scales. That is, in addition to oligomerization on the nanometer scale, receptors are organized into submicron domains. Understanding the relationship between these two phenomena and implications to receptor activation is the subject of the present study.

† A.H.A.C. was a recipient of an R. D. Wright Biomedical Career Development Award from the Australian National Health and Medical Research Council (NHMRC). This work was also supported by Australian NHMRC Project Grant Number 280918.

* Address correspondence to this author at the Ludwig Institute for Cancer Research. Tel: +61-3-341-3158. Fax: +61-3-341-3104. E-mail: andrew.clayton@ludwig.edu.au.

[1] Abbreviations: FRET, fluorescence resonance energy transfer; EGF, epidermal growth factor; EGFR, epidermal growth factor receptor; ICM, image correlation microscopy; FLIM, fluorescence lifetime imaging microscopy.

10.1021/bi700002b CCC: $37.00
Published on Web 03/24/2007

To determine a mechanism of ligand-dependent or ligand-independent receptor activation in a tumor cell environment requires knowledge of the spatial organization of the unligated receptor population on the cell surface. Our studies are designed to (1) probe the distribution of unligated receptor in A431 cells using a ligand-blocking antibody, (2) develop a hybrid microscopy that could distinguish between (a) nanometer scale association independent of higher order clustering, (b) nanometer scale association enhancement in higher order clusters, or (c) nanometer scale association reduction in higher order clusters, and (3) determine the influence of the tyrosine kinase inhibitor AG1478 on the distribution of unligated receptors. To this end we employed lifetime-based FRET microscopy (*11*, *31*) to detect nanometer scale associations, image correlation microscopy to detect higher order clustering on the submicron scale (*4*−*10*), and a hybrid analysis to determine the relationship between the two types of association.

Our analysis, using Alexa488- and Alexa546-labeled anti-EGFR antibody, mAb528, as probes of receptor association in the absence of exogenous ligand suggests that the EGFR is present in at least three different states differing in degree of nanoscale and submicron scale clustering on the surface of A431 cells. The analysis is consistent with tetramers (or higher order oligomers) of unligated EGFR which are assembled in complexes containing a total number of 10−30 receptors on the submicron scale. A pool of lower order clusters (monomers, dimers, or heterooligomers with erb2, -3, or -4 incapable of undergoing FRET) is also present within the FRET clusters and in spatially distinct areas on the cell surface. The observation of higher order clusters in unligated receptors in A431 cells is distinctly different from the situation of EGFR expressed at a normal level in BaF/3 cells wherein EGFR is clustered as lower order clusters (dimers and monomers) in the absence of ligand (*31*). Tyrosine kinase inhibition with AG1478 was shown to disperse the large clusters and alter the orientation and/or separation of the probes on the nanometer scale. These results are consistent with a nascent hierachical receptor organization of the unligated receptor population that can be perturbed by binding of AG1478 in the ATP binding site of the kinase. The ramifications of the results to mechanisms of EGFR activation in a tumor cell environment are discussed.

EXPERIMENTAL PROCEDURES

Preparation of mAb528 Alexa488 and Alexa546 Fluorescent Conjugates. mAb528 was produced and purified to greater that 95% homogeneity by protein A affinity followed by size exclusion chromatography in our Biological Production Facility (Ludwig Institute for Cancer Research, Melbourne, Australia) (*22*). Quality and purity of the antibody were confirmed by SDS−PAGE. mAb528 was directly labeled with AlexaFluor488 or AlexaFluor546 dye using the appropriate monoclonal antibody labeling kit (Molecular Probes/Invitrogen, Melbourne, Australia) according to the manufacturer's instructions. Efficiency of labeling was assessed by determining the moles of dye bound to moles of protein using the formula (A294 × dilution factor)/(extinction coefficient of dye × protein concentration (M)), where the extinction coefficients for AlexaFluor488 and AlexaFluor546 are 71000 and 104000 cm^{-1} M^{-1}, respectively. The fluorophore−antibody conjugates were quality assured for binding to EGFR by using semiquantitative flow cytometry analysis on A431 cells. In all experiments an irrelevant isotype-matched antibody was labeled as above and used to confirm specificity.

Cell Staining and Fixation Protocol for mAb528 Fluorescent Conjugates. Antibodies have the potential to cross-link proteins and influence the multimerization state of the EGFR. To avoid this occurrence, the cells were gently fixed before addition of labeled antibody. A431 cells were seeded into 12-well plates containing 18 mm round glass coverslips and grown overnight. Media were removed, and cells were washed once with phosphate-buffered saline, pH 7.4 (PBS), and fixed for 10 min at room temperature with 4% paraformaldehyde in PBS. After being washed, cells were blocked with 3% human serum albumin in PBS for 30 min and then incubated with different ratios of AlexaFluor488/546-labeled mAb528 for 20 min at room temperature in the dark. Cells were then washed sequentially with PBS, Milli-Q, H_2O, and ethanol before mounting in DPX. Previous studies have shown that this mounting procedure does not significantly perturb the distribution of membrane proteins (*21*).

Laser Scanning Confocal Microscopy. Images representing membrane-associated EGFR were collected using a Bio-Rad MRC 1000 scanning fluorescence confocal microscope (Nikon Plan Apo, 60× NA 1.4 oil immersion lens, zoom = 10, pinhole = 2.4) with FITC emission optics (excitation 488 nm, emission 520/22 nm band-pass). Each image was the accumulation of greater than 50 scans in the photon counting mode.

Fluorescence Lifetime Imaging Microscopy. FLIM experiments were carried out using instrumentation and procedures as outlined previously (*31*).

Image Correlation Microscopy. Spatial autocorrelation analysis (*4*, *40*) of the confocal microscopy images was carried out as previously described (*31*). This analysis yields the average number of clusters per square micron (or cluster density, ⟨CD⟩), which is related to the amplitude of the autocorrelation function [$g(0)$] and the width of the autocorrelation function (ω) by the equation:

$$\langle \mathrm{CD} \rangle = [g(0)(\pi\omega^2)]^{-1} \quad (1)$$

FRET-FLIM-ICS. The qualitative concept of FRET-FLIM-ICS is illustrated schematically in Figure 1. Donor-labeled molecules engaged in nanoscale interactions (FRET) with acceptor-labeled molecules show a distinctly different donor fluorescence lifetime to those not undergoing nanoscale interactions. Using modulated excitation and a phase-sensitive detector, the fluorescence from both FRET molecules and non-FRET molecules can be imaged using FLIM. Because of the different lifetimes of the FRET and non-FRET states, each will have a characteristic intensity profile as a function of phase delay between excitation and detector. The basis of separating the nanoscale- from the nonnanoscale-interacting proteins relies on using a phase-suppression (*12*, *26*) software approach that effectively nullifies the contributions of FRET states from the total, leaving only the emission from the non-FRET molecules and vice versa. This is a generalization of procedures used previously to obtain images of different lifetime states (*38*). Once fluorescence images representing FRET and non-FRET states are separated, these can then be processed using spatial correlation techniques

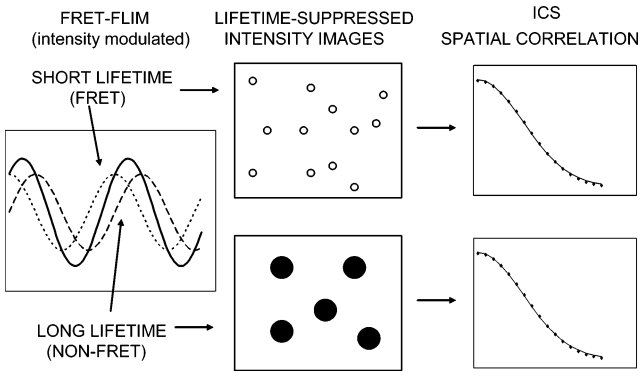

FIGURE 1: Basis of FRET-FLIM-ICS microscopy. Förster resonance energy transfer (FRET) from a donor molecule to an acceptor molecule causes a decrease in the excited-state lifetime of the donor molecule. Phase-modulation methods can separate short- (FRET) and long-lived emitters (non-FRET) on the basis of their differing phase and modulation. When taken into the cell and imaged by fluorescence lifetime imaging microscopy (FLIM), the fluorescence contributions from the FRET and non-FRET states can be separated. Spatial correlation methods, image correlation spectroscopy (ICS), can then be applied to the FRET and non-FRET images to yield the density of FRET and non-FRET clusters, the relative degree of aggregation of the FRET and non-FRET clusters, and the degree of spatial correlation between the FRET and non-FRET clusters.

(*4*−*10*, *19*) to determine the cluster density, the degree of association ratio, and the degree of spatial correlation between FRET and non-FRET molecules.

The protocol for determining the FRET and non-FRET resolved parameters is given below. A detailed discussion is given in the Supporting Information. Only the key equations are given here.

Separate FRET from non-FRET states and represent as FRET-associated and non-FRET-associated fluorescence images.

The fractional fluorescence due to the FRET signal at each pixel is given by (*26*)

$$\beta(x,y) = [M^{\mathrm{TOT}}\cos(\phi)(x,y) - M^{\mathrm{non-FRET}}\cos(\phi)]/ [M^{\mathrm{FRET}}\cos(\phi) - M^{\mathrm{non-FRET}}\cos(\phi)] \quad (2)$$

where $M^{\mathrm{non-FRET}}\cos(\phi)$ and $M^{\mathrm{FRET}}\cos(\phi)$ denote the cosine transforms characteristic of the non-FRET and FRET states and are constants.

The FRET-associated fluorescence image $[I(x,y)^{\mathrm{FRET}}]$ is obtained by multiplying the fractional fluorescence due to FRET at each pixel $[\beta(x,y)]$ by the total fluorescence at each pixel, i.e.

$$I(x,y)^{\mathrm{FRET}} = \beta(x,y)I(x,y)^{\mathrm{TOT}} \quad (3)$$

$$I(x,y)^{\mathrm{non-FRET}} = [1 - \beta(x,y)]I(x,y)^{\mathrm{TOT}} \quad (4)$$

The procedure is similar for the non-FRET states (see eq 4).

From these images the mean FRET and non-FRET fluorescence can be obtained.

Calculation of the Ratio of the Degree of Aggregation of FRET Clusters to Non-FRET Clusters. Spatial autocorrelation analysis (eq 1) on the fluorescence images representing FRET and non-FRET states yields the cluster density of the FRET states (CD^{FRET}) and the cluster density of the non-FRET ($CD^{\mathrm{non-FRET}}$) states. Together with the mean intensity of FRET ($\langle I\rangle^{\mathrm{FRET}}$) and non-FRET fluorescence ($\langle I\rangle^{\mathrm{non-FRET}}$), the degree of aggregation ratio can be calculated:

$$DA^{\mathrm{FRET}}/DA^{\mathrm{non-FRET}} = \gamma(\langle I\rangle^{\mathrm{FRET}}CD^{\mathrm{non-FRET}}/ \langle I\rangle^{\mathrm{non-FRET}}CD^{\mathrm{FRET}}) \quad (5)$$

where γ = lifetime of non-FRET/lifetime of FRET.

Spatial cross-correlation analysis between images representing FRET and non-FRET states yields the degree of spatial correlation between FRET and non-FRET states. The density of clusters containing both FRET and non-FRET states is given by (*19*)

$$CD^{\mathrm{non-FRET/FRET}} = CD^{\mathrm{non-FRET}}g(0)^{\mathrm{non-FRET/FRET}}/g(0)^{\mathrm{FRET}} \quad (6)$$

Classification Scheme Based on FRET-FLIM-ICS. In the context of lateral organization of membrane proteins the FRET-FLIM-ICS parameters can be used to broadly classify the nanoscale and submicron scale associations of membrane proteins. A general, but necessarily approximate, model must incorporate dim (small) and bright (large) submicron scale clusters as well as the presence of nanoscale associations in some or all of the clusters. Three main types of lateral organization are possible:

Class I: nanoscale (FRET) associations have equal probability in small and large submicron scale clusters:

$$CD^{\mathrm{non-FRET/FRET}} = CD^{\mathrm{FRET}} = CD^{\mathrm{non-FRET}}$$

Class II: nanoscale associations (FRET) are enhanced in large clusters relative to small clusters:

$$DA^{\mathrm{FRET}}/DA^{\mathrm{non-FRET}} > 1$$

Class III: nanoscale associations (FRET) are reduced in large clusters relative to small clusters:

$$DA^{\mathrm{FRET}}/DA^{\mathrm{non-FRET}} < 1$$

RESULTS

EGFR Clustering on the Submicron Scale. Image correlation microscopy has been used previously to determine the aggregation states of immunotagged EGFR on the surface of A431 cells which overexpress the EGFR [$(1-3) \times 10^6$ receptors]. The results indicated that the total EGFR population is highly clustered (cluster densities = 10−19 clusters per square micron and degree of aggregation = 10−33 receptors per cluster) on the submicron scale (*19*). We used image correlation spectroscopy to determine the submicron scale clustering and average degree of aggregation of the unligated EGFR population using fluorescently tagged mAb528. Monoclonal antibody 528 (*28*) has been used as a competitive antibody for EGF binding to the human EGFR and binds specifically to the L2 domain (domain 3) on the extracellular domain of the receptor. Figure 2A shows the characteristic membrane staining for EGFR in A431 cells labeled with the mAb528−Alexa488 conjugate. Figure 2B illustrates a typical membrane section of an A431 cell stained with Alexa488−mAb528 obtained at high magnification and Figure 2C the corresponding computed autocorrelation function. The average density of clusters was 32 ± 9 per square micron (n = 6), and the correlation function width

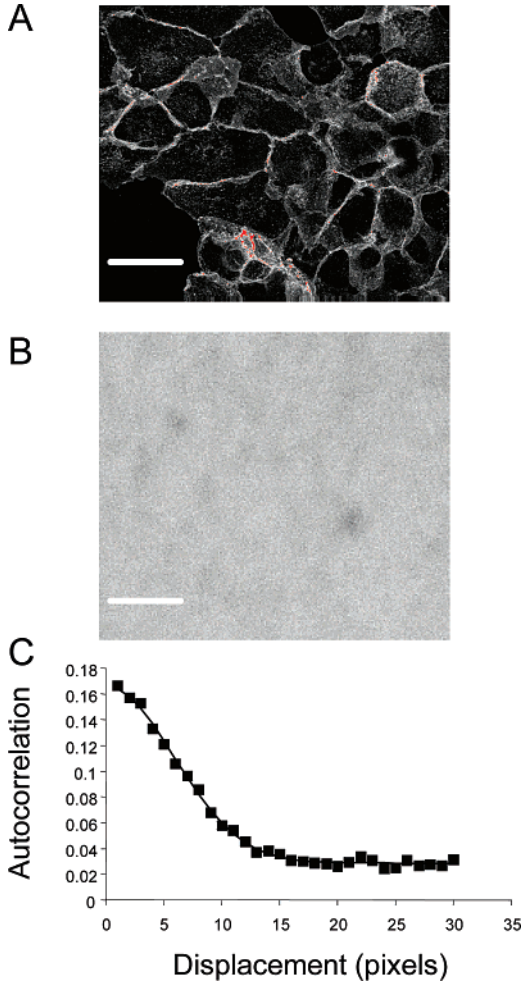

FIGURE 2: (A) Confocal image of EGFR immunotagged with mAb528−Alexa488 on A431 cells. The image represents a maximum intensity projection of a 3D stack. The scale bar length represents 40 μm. (B) High-resolution confocal image of EGFR immunotagged with mAb528−Alexa488 (photon count detection). This image is an optical section taken at the apical membrane of an A431 cell and at high zoom. The scale bar length represents 1.5 μm. (C) Spatial autocorrelation function. Typical 1D autocorrelation function of cell surface immunotagged EGFR: squares, experimental; solid line, fit to Gaussian plus offset function. The peak of the autocorrelation function is used to compute the cluster density.

was 0.3−0.35 μm. On the basis of an average expression level of (1−3) $\times$ 10^6 EGFR and a cell surface area of 3000 square microns (*19*), we calculate an average degree of aggregation of 10−30 receptors per cluster. The image correlation results provide evidence for spatially correlated clusters of EGFR's on the submicron scale but do not directly reveal the cluster size distribution or organization of receptors within or outside the clusters on the nanometer scale.

Nanoscale Clustering of Unligated EGFR. To test for the presence of fluorophore−fluorophore interactions due to oligomerization of the unligated EGFR on the nanometer scale, we measured FRET between the Alexa488−mAb528 donor and the Alexa546−mAb528 acceptor on the A431 cells using FLIM. Figure 3A illustrates the fluorescence and lifetime images of A431 stained with Alexa488−mAb528. The distributions of phase lifetimes for the donor-only cell and for donor-and-acceptor cell are also shown in the histograms in Figure 3A. The intensity image of the donor shows prominent staining of the EGFR at the membrane and at the sites of cell-to-cell contact. The donor lifetime image shows a relatively uniform spatial lifetime distribution at the resolution of the camera employed, as also revealed by the tight distribution of lifetimes in the donor histogram. Clear evidence of FRET can be seen by the shift of the donor-detected lifetime histogram (3.1 $\pm$ 0.2 ns) to a shorter value in the presence of acceptor (2.7 $\pm$ 0.2 ns).

The results from FRET-FLIM experiments carried out at several acceptor:donor mole ratios are depicted in Figure 3B. The data are represented using the AB-plot process (*26*). For a simple two-component system (i.e., monomer−dimer equilibrium) the AB plot should conform to a linear relationship (*26*) because only two donor states (donor−donor and donor−acceptor) are present in such a system. A nonlinear plot would imply that FRET occurs within EGFR complexes containing more than two differently labeled antibodies. We have approached analysis of the FRET-FLIM AB plot using two different theoretical models as detailed in the Supporting Information. In the context of a simple oligomer model, the tetramer model (Figure 3B, right panel, with 90% tetramer and 10% non-FRET fluorescence) shows an improved fit compared to a monomer−dimer model [Figure 3B, left panel (eqs S16−S20)]. In the second model, the two-compartment quenching model, there is a fraction of Alexa488−mAbs inaccessible to FRET quenching by Alexa546−mAb (monomers or oligomers with unfavorable FRET geometries) and a distinct fraction which is accessible to FRET quenching by acceptor−mAb528. This model can account for the curved AB plot and yields a quenchable fraction of 66% and a nonquenchable fraction of 33%. However, a random association of monomers within the quenchable fraction is not consistent with the data. This suggests that the receptor is nonrandomly clustered as higher order oligomers.

Relationship between Nanoscale and Submicron Scale Clustering of Unligated EGFR. Together, ICS and FRET-FLIM measurements reveal that the EGFR is clustered to some degree on the nanometer and submicron scales. In this scenario, there are three possible types of lateral organization of the receptor. In the class I model, oligomerization and submicron scale clustering are independent, in which case larger scale clusters are built from nanoscale clusters. In another model, class II, EGFR nanoscale self-association is enhanced in the large clusters and reduced in small clusters; that is, there is a correlation between nanoscale self-association and higher order clustering. In the class III model, EGFR nanoscale self-association is reduced in the large-scale clusters and enhanced in the regions outside the large clusters. We now show that it is possible to obtain information about the lateral distribution from a measurement on a single cell or region thereof. Figure 4 represents fluorescence images from a region on the A431 cell surface corresponding to FRET, non-FRET, and total fluorescence obtained by analysis of the FLIM data as outlined in Experimental Procedures (eqs 1−3; see also Supporting Information). Figure 5 displays the autocorrelation functions obtained from fluorescence images of the FRET and non-FRET states and the cross-correlation function between the FRET and non-FRET fluorescence images. Table 1 details the corresponding computed correlation parameters obtained from the correlation function amplitudes $\langle g(0)\rangle$ (eqs 1), the mean cluster densities ($\langle$CD$\rangle$), and the average image intensities ($\langle I\rangle$). We

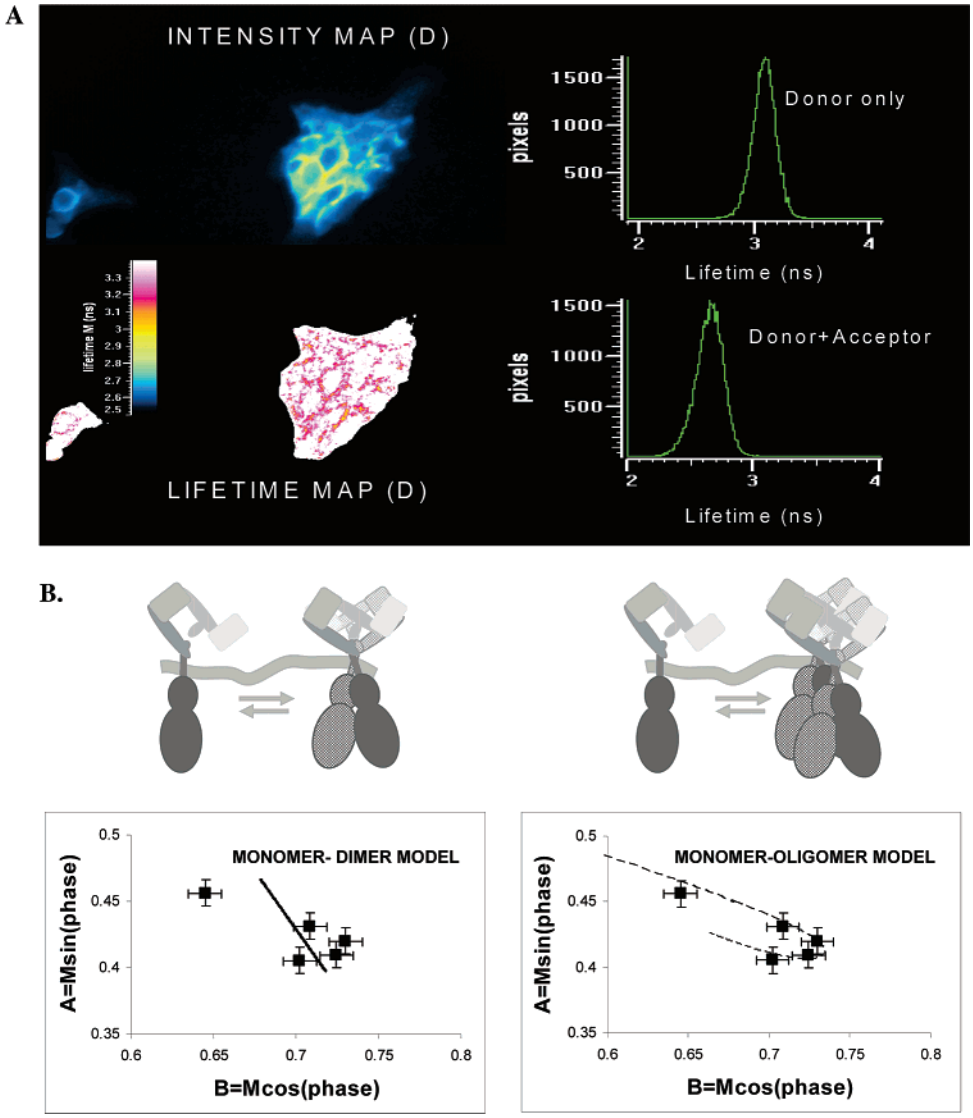

FIGURE 3: Fluorescence lifetime imaging microscopy detected FRET (FRET-FLIM) between mAb528−Alexa488 and mAb528−Alexa546 bound to EGFR on the surface of A431 cells. (A) Images represent fluorescence intensity of mAb528−Alexa488 (left top) and mAb528−Alexa488 phase lifetime (left bottom). The histograms represent the pixel-by-pixel frequencies of lifetimes obtained in the absence (right upper) and presence (right lower) of the mAb528−Alexa546 acceptor (2:1 mole ratio). (B) FRET-FLIM data plotted in AB-plot form. *X*-axis: B = Mcos(phase). *Y*-axis: A = Msin(phase). Each data point represents the average of three FLIM measurements at a fixed donor:acceptor ratio (ratios used were 0, 1, 2, 3, and 5). Left panels: Dimer schematic and fit to dimer model (two lifetime states, solid line). Right panels: Oligomer schematic and fit to an oligomer model (four lifetime states, dotted line).

note that the cluster densities in the present case are apparent quantities because they are obtained under conditions where the cell is labeled with 33% Alexa488−mAb528 and 66% Alexa546−mAb528 and hence not saturated with donor-labeled antibody. The degree of aggregation ratio (eq 5) and the cross-correlation parameters are ratiometric or relative quantities (eq 6) and hence provide more reliable information about the underlying cell surface distribution, since these quantities are independent of the total number of receptors sampled in the subimage. From the computed degree of aggregation ratio (eq 5) it is apparent that the FRET states are included in clusters that contain between 7- and 11-fold more receptor than the non-FRET states. In the context of a simple monomer−oligomer/bimodal FRET/non-FRET model that takes into account the competitive donor/acceptor labeling, the degree of aggregation ratio can be used to derive estimates of the aggregate size of the oligomeric population (see Supporting Information). With this model, FRET states are in higher order clusters containing on average 15−30 receptors per cluster. The density of cross-correlated clusters ($CD^{FRET/non-FRET}$, eq 6) is 13 ± 5 clusters per square micron and is similar to the density of FRET clusters (9 ± 1 clusters per square micron) but is lower than the non-FRET states (36 ± 7 clusters per square micron). Thus every FRET molecule cluster is colocalized with a non-FRET molecule cluster but only about one-third of all non-FRET molecules are colocalized with a FRET molecule. The results are qualitatively consistent with a lateral organization where there is a minor population of monomers and/or small oligomers not undergoing FRET and a major distribution of larger clusters containing both FRET and non-FRET molecules. This is a class II model.

Binding of the Kinase Inhibitor AG1478 Alters Small-Scale and Large-Scale Clustering of Unligated EGFR. The effect of pretreating the cells with AG1478, a specific inhibitor of the intracellular EGFR kinase domain, on the spatial

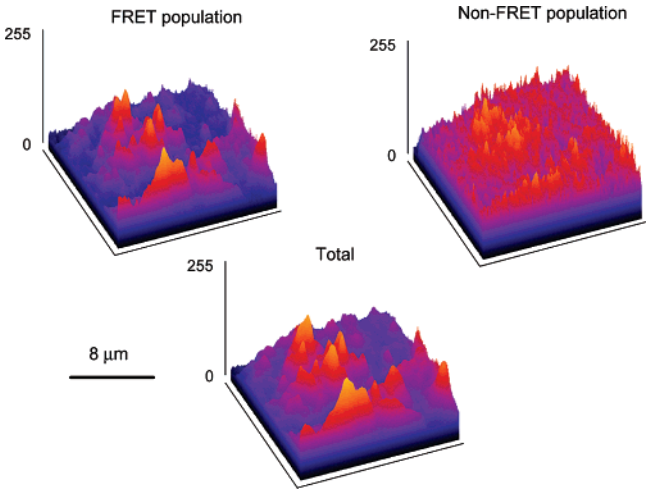

FIGURE 4: FRET-FLIM-based decomposition of fluorescence images of mAb528−Alexa488−EGFR (in the presence of 2-fold Alexa546−mAb528) into FRET, non-FRET, and total states.

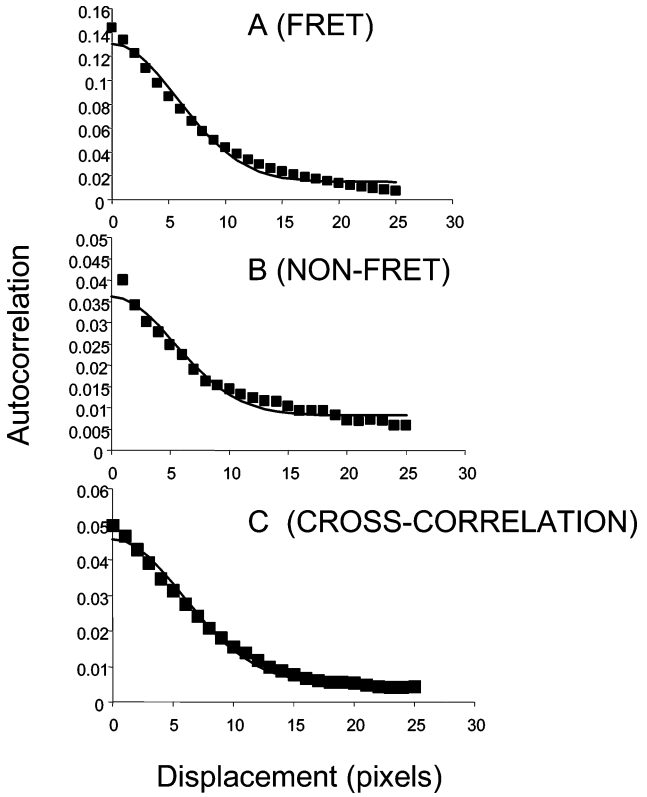

FIGURE 5: FRET-FLIM-ICS. Spatial auto- and cross-correlation functions of the images presented in Figure 4. (A) Autocorrelation function of fluorescence from FRET states. The amplitude of the function is used to compute the cluster density of FRET molecules. (B) Autocorrelation function of fluorescence from non-FRET states. The amplitude of the function is used to compute the cluster density of non-FRET molecules. (C) Spatial cross-correlation function between FRET and non-FRET states. The amplitude of the function is proportional to the density of clusters containing both FRET and non-FRET molecules.

organization of the unligated EGFR was determined using ICS and FRET-FLIM as described above. The average density of clusters in the presence of AG1478 was 88 ± 15 clusters per square micron ($n = 6$) compared with 32 ± 9 clusters per square micron ($n = 6$) for the untreated cells. Since the cell surface expression level is only slightly increased (<25%) with AG1478 binding, the large increase in cluster density must be due to a reduced number of receptors per cluster (i.e., 4−10 receptors per cluster). FLIM experiments with AlexaFluor488−mAb528 alone and in the presence of AlexaFluor546−mAb528 (acceptor:donor ratio, 2:1) revealed an undetectable change in AlexaFluor488 lifetime in the presence of the AlexaFluor546−mAb528 acceptor (see Supporting Information). Thus, AG1478 binding and kinase inhibition alter the nanoscale and submicron scale interactions sensed by probes located on the unligated extracellular domain of the receptor.

Table 1: FRET-FLIM-ICM Microscopy[a] Parameters for A431 Cell Surface Immunotagged with Alexa488/Alexa546−mAb528 (2:1 Acceptor:Donor Ratio)

analysis	$\langle I \rangle$	$\langle g(0) \rangle$	$\langle \mathrm{CD} \rangle^b$	$\langle \omega \rangle^d$
total	865	0.0748	13.4 ± 2	0.55
FRET population	608	0.1107	9.0 ± 1	0.55
non-FRET population	257	0.0279	35.9 ± 7	0.50
cross-correlation[c]	na	0.0404	13.1 ± 5	0.53
degree of association ratio	na	9.4 ± 2	na	na

[a] Microscope: LED excitation, 470 nm, and emission, 520−560 nm. [b] ⟨CD⟩, mean number of clusters per square micron. [c] Cross-correlation $= \mathrm{CD}^{\mathrm{non-FRET/FRET}} = \mathrm{CD}^{\mathrm{non-FRET}} g(0)^{\mathrm{non-FRET/FRET}} / g(0)^{\mathrm{FRET}}$. [d] ⟨$\omega$⟩, width of correlation function (in microns).

DISCUSSION

To our knowledge this study represents the first detailed examination of the association states of the unligated forms of EGF receptor on the A431 cell surface. Our findings unify previous studies by (a) determining the average number of receptors associated at the sub-10 nm scale and (b) specifically addressing the relationship between the nanoscale (FRET) oligomers (*18*) and spatially correlated submicron scale clusters observed by ICS (*19*). The analysis is consistent with higher order oligomers of unligated EGFR (average number associated on the nanometer scale of 4) which are assembled in complexes containing a total number of 10−30 receptors on the submicron scale. The nanoscale associations within the higher order clusters are neither random nor homogeneous. A pool of lower order clusters [monomers, dimers, or heterooligomers (with erb2, -3, or -4) incapable of undergoing FRET] is also present within the FRET clusters and in spatially distinct areas on the cell surface. It is estimated that only a small fraction of the total receptor population is outside the larger clusters (<10%). Although our interpretation is constrained by the simple aggregation models employed, our results point to a distribution of EGFR states that differ in aggregate size, aggregate density, and length scale of association (<10 versus >10 nm).

Biochemical studies addressing the localization of the receptor suggest that in unstimulated cells the majority of EGFR's are localized to noncaveolar lipid raft domains (*33*), which could potentially form sites of enhanced association. Chemical cross-linking studies in cell lines overexpressing the EGFR have demonstrated the presence of monomers, dimers, and high-order oligomers in the absence of added ligand (*39*). Our FRET analysis reveals that the higher order oligomerization occurs on the intact A431 cell surface, within submicron clusters, and in the absence of exogenous ligand.

It is tempting to interpret the nanoscale associations of the mAb528−EGFR complex in terms of a recently reported structure of a related antibody complex, the C225−EGFR

complex (*29*). C225 binds a similar region of the receptor as mAb528 and, like mAb528, partially blocks ligand binding. The structure of the C225 antibody in complex with EGFR shows that the antibody binds to a monomeric form of the EGFR in a tethered configuration. By reference to the structural data of the EGFR−C225 complex, it follows that unligated and tethered mAb528−EGFR is capable of forming oligomers [with itself or other erbB molecules (*35*)] via a non-back-to-back dimer interface(s) at the cell surface (in a side-by-side and/or head-to-head arrangement). Alternatively, the environment inside the clusters may be permissive for partial untethering of the receptor, in which case a back-to-back dimerization interface, in addition to other interfaces, may be engaged. A third possibility is that nonrandom accumulation of mAb528−EGFR in domains of high local concentration mediated via specialized cell structures [lipid rafts, caveolin, or cytoskeleton (*33*)] facilitates EGFR oligomerization into the distance range for FRET to occur. A detailed interpretation awaits the availability of 3D structural models of unligated erbB dimers and higher order oligomers.

The interesting finding from the present study is that the nanoscale and submicron scale arrangement of the unligated receptors is perturbed by the binding of AG1478 to the intracellular kinase domain. That is, there is a causal link between basal kinase activation and the receptor associations (cluster occupancy and length scale of association). This suggests that higher order associations may play an important role in basal activation in A431 cells in the absence of endogenous ligand. In the biochemical study of Zhu and coworkers (*39*) EGFR overexpression was correlated with a monotonic but nonlinear increase in ligand-independent kinase activation and phosphorylation. Two models were proposed to explain these observations. In the first model, overexpression increases the proportion of ligand-free dimers that interconvert between active and inactive forms. Kinase inhibition (at constant receptor expression level) in this case would favor the inactive conformation but would not change the cluster size or oligomerization state. In the second model, EGFR overexpression drives the formation of a ligand-free tetramer, which activates the kinase. According to this hypothesis, inhibition of kinase activation would favor the kinase inactive dimer and/or monomeric form(s) and thus lead to dispersal of the EGFR oligomers and clusters. The significance of understanding the oligomeric and conformational states of the EGFR in the presence of AG1478 is underscored by a recent study demonstrating that AG1478 alters the conformation of EGFR dimers, allowing the binding of an antibody with enhanced therapeutic potential (*47*).

Clustering and higher order oligomerization of unliganded receptors have been reported for other members of the EGFR family. Jovin and colleagues have observed activation-dependent higher order clusters of erbB2 using scanning near-field optical microscopy in cells overexpressing erbB2 on the submicron scale (*21*). In the Jovin study an increase in diameter of the erbB2-containing clusters was correlated with cellular activation (by antibodies or ligands). This effect could be inhibited by tyrosine kinase inhibitors. Landgraf has reported ligand-free higher order oligomers formed from isolated extracellular domains of the erbB3 system in solution that can be disrupted to form dimers in the presence of ligand (*43*). These results were interpreted as a result of having at least two oligomerization interfaces (*43*).

Using similar biophysical techniques, we recently reported a dimer-to-tetramer transition following ligand binding in cells expressing a normal level of EGFR (*31*). Image correlation microscopy of EGFR−eGFP in BaF/3 cells revealed an average number of receptors per cluster of 2.2 increasing to 3.7 receptors per cluster in the presence of EGF (*31*). Ligand-based FRET was used to confirm a nanoscale association of two ligated dimers to form a side-by-side or slightly staggered tetrameric complex (*31*). At the low expression level of these cells (50000 receptors per cell) ligand-independent tetramer formation is at a low level, and ligand is needed to drive the association of monomers and/or dimers to form an active higher order complex. Diffusion of receptors is required as part of the activation process in these cells. However, the even higher order association of receptors on the submicron and nanometer scales in the A431 cells suggests a fundamentally different mode of ligand-induced activation of the receptor in this cell type.

What are the implications of higher order preclustering on the mechanism of activation? Higher order oligomerization between receptors on the nanometer scale is predicted to enhance the sensitivity of receptors to changes in ligand concentration (*45*, *46*) and give rise to long-range conformational spread (*45*), effects that would be absent or diminished if the receptors existed as isolated monomers or dimers at low density on the cell surface. Numerical simulations suggest that packing the EGFR into domains of high local density as well as domains in which the receptor is more diffusely arranged produces concave-up Scatchard plots for ligand binding (*42*). The sensitivity of ligand binding to changes in ligand concentration can also be enhanced by a factor of N, where N is the number of subunits in a cooperative oligomer (*45*).

Long-range conformational spread may play a role in spread of activation and phosphorylation observed for EGFR in overexpressing cells but not in cells that express a normal receptor level (*27*, *44*). The close packing of multiple receptors in the absence of exogenous ligand, a feature of EGFR overexpression revealed in the present study, may allow for the conformational spread (*46*) and/or short-range diffusion (*41*) promoting activation across multiple receptors once stimulated locally by ligand without the requirement for long-range diffusion.

Work is in progress to extend the multimodal imaging techniques presented here to elucidate the connections between receptor cell surface organization, receptor dynamics, and the activation, progression, attenuation, and therapeutic intervention of signaling cascades.

SUPPORTING INFORMATION AVAILABLE

A theory of FRET-FLIM-ICS and a discussion of the advantages and disadvantages of the technique and equations relevant to the analysis of FRET-FLIM data in terms of oligomer and two-compartment quenching models. This material is available free of charge via the Internet at http://pubs.acs.org.

REFERENCES

1. Citri, A., and Yarden, Y. (2006) EGF-ERBB signalling: towards the systems level, *Nat. Rev. Mol. Cell Biol. 7*, 505−516.

2. Yarden, Y., and Schlessinger, J. (1987) Self-phosphorylation of epidermal growth factor receptor: evidence for a model of intermolecular allosteric activation, *Biochemistry 26*, 1434−1442.
3. Vereb, G., Szollosi, J., Matko, J., Nagy, P., Farkas, T., Vigh, L., Matyus, L., Waldmann, T. A., and Damjanovich, S. (2003) Dynamic, yet structured: The cell membrane three decades after the Singer-Nicolson model, *Proc. Natl. Acad. Sci. U.S.A. 100*, 8053−8058.
4. Peterson, N. O. (1986) Scanning fluorescence correlation spectroscopy. I. Theory and simulation of aggregation measurements, *Biophys. J. 49*, 809−815.
5. Medina, M. A., and Schwille, P. (2002) Fluorescence correlation spectroscopy for the detection and study of single molecules in biology, *BioEssays 24*, 758−764.
6. Hebert, B., Costantino, S., and Wiseman, P. W. (2005) Spatiotemporal image correlation spectroscopy (STICS) theory, verification, and application to protein velocity mapping in living CHO cells, *Biophys. J. 88*, 3601−3614.
7. Palmer, A. G., III, and Thompson, N. L. (1989) High-order fluorescence fluctuation analysis of model protein clusters, *Proc. Natl. Acad. Sci. U.S.A. 86*, 6148−6152.
8. Chen, Y., Muller, J. D., So, P. T., and Gratton, E. (1999) The photon counting histogram in fluorescence fluctuation spectroscopy, *Biophys. J. 177*, 553−567.
9. Qian, H., and Elson, E. L. (1990) Distribution of molecular aggregation by analysis of fluctuation moments, *Proc. Natl. Acad. Sci. U.S.A. 87*, 5479−5483.
10. Berland, K. M., So, P. T., and Gratton, E. (1995) Two-photon fluorescence correlation spectroscopy: method and application to the intracellular environment, *Biophys. J. 68*, 694−701.
11. Jares-Erijman, E. A., and Jovin, T. M. (2003) FRET imaging, *Nat. Biotechnol. 21*, 1387−1395.
12. Gratton, E., Jameson, D. M., and Hall, R. D. (1984) Multifrequency phase and modulation fluorometry, *Annu. Rev. Biophys. Bioeng. 13*, 105−124.
13. Yarden, Y., and Sliwkowski, M. X. (2001) Untangling the ErbB signalling network, *Nat. Rev. Mol. Cell Biol. 2*, 127−137.
14. Jorissen, R. N., Walker, F., Pouliot, N., Garrett, T. P., Ward, C. W., and Burgess, A. W. (2003) Epidermal growth factor receptor: mechanisms of activation and signalling, *Exp. Cell Res. 284*, 31−53.
15. Garrett, T. P., McKern, N. M., Lou, M., Elleman, T. C., Adams, T. E., Lovrecz, G. O., Zhu, H. J., Walker, F., Frenkel, M. J., Hoyne, P. A., Jorissen, R. N., Nice, E. C., Burgess, A. W., and Ward, C. W. (2002) Crystal structure of a truncated epidermal growth factor receptor extracellular domain bound to transforming growth factor alpha, *Cell 110*, 763−773.
16. Moriki, T., Maruyama, H., and Maruyama, I. N. (2001) Activation of preformed EGF receptor dimers by ligand-induced rotation of the transmembrane domain, *J. Mol. Biol. 311*, 1011−1026.
17. Sako, Y., Minoghchi, S., and Yanagida, T. (2000) Single-molecule imaging of EGFR signalling on the surface of living cells, *Nat. Cell Biol. 2*, 168−172.
18. Gadella, T. W., Jr., and Jovin, T. M. (1995) Oligomerization of epidermal growth factor receptors on A431 cells studied by time-resolved fluorescence imaging microscopy. A stereochemical model for tyrosine kinase receptor activation, *J. Cell Biol. 129*, 1543−1558.
19. Petersen, N., Brown, C., Kaminski, A., Rocheleau, J., Srivastava, M., and Wiseman, P. W. (1998) Analysis of membrane protein cluster densities and sizes in situ by image correlation spectroscopy, *Faraday Discuss. 111*, 289−305.
20. Zidovetzki, R., Yarden, Y., Schlessinger, J., and Jovin, T. M. (1981) Rotational diffusion of epidermal growth factor complexed to cell surface receptors reflects rapid microaggregation and endocytosis of occupied receptors, *Proc. Natl. Acad. Sci. U.S.A. 78*, 6981−6985.
21. Nagy, P., Jenei, A., Kirsch, A. K., Szollosi, J., Damjanovich, S., and Jovin, T. M. (1999) Activation-dependent clustering of the erbB2 receptor tyrosine kinase detected by scanning near-field optical microscopy, *J. Cell Sci. 112*, 1733−1741.
22. Masui, H., Kawamoto, T., Sato, J. D., Wolf, B., Sato, G., and Mendelsohn, J. (1984) Growth inhibition of human tumor cells in athymic mice by anti-epidermal growth factor receptor monoclonal antibodies, *Cancer Res. 44*, 1002−1007.
23. Hanley, Q. S., and Clayton, A. H. A. (2005) AB-plot assisted determination of fluorophore mixtures in a fluorescence lifetime microscope using spectra or quenchers, *J. Microsc. 218*, 62−67.
24. van Munster, E. B., and Gadella, T. W., Jr. (2004) Suppression of photobleaching-induced artifacts in frequency-domain FLIM by permutation of the recording order, *Cytometry 58A*, 185−194.
25. Magde, D., Rojas, G. E., and Seybold, P. G. (1999) Solvent dependence of the fluorescence lifetimes of xanthene dyes, *Photochem. Photobiol. 70*, 737−744.
26. Clayton, A. H. A., Hanley, Q. S., and Verveer, P. J. (2004) Graphical representation and multicomponent analysis of single-frequency fluorescence lifetime imaging microscopy data, *J. Microsc. 213*, 1−5.
27. Verveer, P. J., Wouters, F. S., Reynolds, A. R., and Bastiaens, P. I. (2000) Quantitative imaging of lateral ErbB1 receptor signal propagation in the plasma membrane, *Science 290*, 1567−1570.
28. Gill, G. N., Kawamoto, T., Cochet, C., Le, A., Sato, J. D., Masui, H., McLeod, C., and Mendelsohn, J. (1984) Monoclonal anti-epidermal growth factor receptor antibodies which are inhibitors of epidermal growth factor binding and antagonists of epidermal growth factor binding and antagonists of epidermal growth factor-stimulated tyrosine protein kinase activity, *J. Biol. Chem. 259*, 7755−7760.
29. Li, S., Schmitz, K. R., Jeffrey, P. D., Wiltzius, J. J. W., Kussie, P., and Ferguson, K. M. (2005) Structural basis for inhibition of the epidermal growth factor receptor by cetuximab, *Cancer Cell 7*, 301−311.
30. Stein, R. A., Hustedt, E. J., Staros, J. V., and Beth, A. H. (2002) Rotational dynamics of the epidermal growth factor receptor, *Biochemistry 41*, 1957−1964.
31. Clayton, A. H. A., Walker, F., Orchard, S. G., Henderson, C., Fuchs, D., Rothacker, J., Nice, E. C., and Burgess, A. W. (2005) Ligand-induced dimer-tetramer transition during activation of the cell surface epidermal growth factor receptor, *J. Biol. Chem. 280*, 30392−30399.
32. Whitson, K. B., Beechem, J. M., Beth, A. H., and Staros, J. V. (2004) Preparation and characterization of Alexa Fluor 594-labeled epidermal growth factor for fluorescence resonance energy transfer studies: application to the epidermal growth factor receptor, *Anal. Biochem. 324*, 227−236.
33. Pike, L. J. (2005) Growth factor receptors, lipid rafts and caveolae: An evolving story, *Biochim. Biophys. Acta 1746*, 260−273.
34. Kenworthy, A. K., and Edidin, M. (1998) Distribution of a glycosylphosphatidylinositol-anchored protein at the apical surface of MDCK cells examined at a resolution of <100 Å using imaging fluorescence resonance energy transfer, *J. Cell Biol. 142*, 69−84.
35. Stoll, S. W., Kansra, S., Peshick, S., Fry, D. W., Leopold, W. R., Wiesen, J. F., Sibilia, M., Zhang, T., Werb, Z., Derynck, R., Wagner, E. F., and Elder, J. T. (2001) Differential utilization and localization of ErbB receptor tyrosine kinases in skin compared to normal and malignant keratinocytes, *Neoplasia 3*, 339−350.
36. Lamb, D. C., Schenk, A., Rocker, C., Scalfi-Happ, C., and Nienhaus, G. U. (2000) Sensitivity enhancement in fluorescence correlation spectroscopy of multiple species using time-gated detection, *Biophys. J. 79*, 1129−1138.
37. Lakowicz, J. R., and Balter, A. (1982) Theory of phase-modulation fluorescence spectroscopy for excited-state processes, *Biophys. Chem. 16*, 99−115.
38. Pepperkok, R., Squire, A., Geley, S., and Bastiaens, P. I. (1999) Simultaneous detection of multiple green fluorescent proteins in live cells by fluorescence lifetime imaging microscopy, *Curr. Biol. 9*, 269−272.
39. Zhu, H. J., Iaria, J., Orchard, S., Walker, F., and Burgess, A. W. (2003) Epidermal growth factor receptor: association of extracellular domain negatively regulates intracellular kinase activation in the absence of ligand, *Growth Factors 21*, 15−30.
40. Costantino, S., Comeau, J. W., Kolin, D. L., and Wiseman, P. W. (2005) Accuracy and dynamic range of spatial image correlation and cross-correlation spectroscopy, *Biophys. J. 89*, 1251−1260.
41. Mayawala, K., Vlachos, D. G., and Edwards, J. S. (2006) Spatial modeling of dimerization reaction dynamics in the plasma membrane: Monte Carlo vs. continuum differential equations, *Biophys. Chem. 121*, 194−208.
42. Mayawala, K., Vlachos, D. G., and Edwards, J. S. (2005) Heterogeneities in EGF receptor density at the cell surface can lead to concave up scatchard plot of EGF binding, *FEBS Lett. 579*, 3043−3047.

43. Kani, K., Warren, C. M., Kaddis, C. S., Loo, J. A., and Landgraf, R. (2005) Oligomers of ERBB3 have two distinct interfaces that differ in their sensitivity to disruption by heregulin, *J. Biol. Chem. 280*, 8238−8247.
44. Sawano, A., Takayama, S., Matsuda, M., and Miyawaki, A. (2002) Lateral propagation of EGF signaling after local stimulation is dependent on receptor density, *Dev. Cell 3*, 245−257.
45. Bray, D., and Duke, T. (2004) Conformational spread: the propagation of allosteric states in large multiprotein complexes, *Annu. Rev. Biophys. Biomol. Struct. 33*, 53−73.
46. Duke, T. A., and Bray, D. (1999) Heightened sensitivity of a lattice of membrane receptors, *Proc. Natl. Acad. Sci. U.S.A. 96*, 10104−10108.
47. Gan, H. K., Walker, F., Burgess, A. W., Scott, A. M., and Johns, T. G. (2007) The EGFR tyrosine kinase inhibitor AG1478 increases the formation of inactive untethered EGFR dimers: Implications for combination therapy with mAb 806, *J. Biol. Chem. 282*, 2840−2850.

BI700002B